Exploring the Spinning and Operations of Multibore Hollow Fiber Membranes for Vacuum Membrane Distillation

Peng Wang and Tai-Shung Chung
Dept. of Chemical and Biomolecular Engineering, National University of Singapore, Singapore 117576, Singapore

DOI 10.1002/aic.14323
Published online December 26, 2013 in Wiley Online Library (wileyonlinelibrary.com)

Hollow fiber membranes with a multibore configuration have demonstrated their advantages with high mechanical strength, easy module fabrication, and excellent stability for membrane distillation (MD). In this work, the microstructure of multibore fibers was optimized for vacuum MD (VMD). A microstructure consisting of a tight liquid contact surface and a fully porous cross-section is proposed and fabricated to maximize the wetting resistance and VMD desalination performance. The new membrane exhibited a high VMD flux of 71.8 L m^{-2} h^{-1} with a 78°C model seawater feed. Investigations were also carried to examine various effects of VMD operational conditions on desalination performance. The 7-bore membrane showed higher flux and superior thermal efficiency under the VMD configuration than the direct contact MD configuration. Different from the traditional single-bore hollow fiber, the VMD flux of multibore membrane at the lumen-side feed configuration was higher than that of the shell-side feed due to the additional evaporation surface of multibore geometry. *AIChE J*, 60: 1078–1090, 2014
Keywords: vacuum membrane distillation, multibore hollow fiber, polyvinylidene fluoride membrane, mechanical strength, highly asymmetric structure

Introduction

Membrane distillation (MD) is an emerging separation technology based on the mechanism of liquid/vapor equilibrium and the transportation of volatile compounds.[1,2] The potential applications of MD have been extensively studied, including seawater desalination, wastewater treatment, concentration of ions and colloids, removal of volatile organic compounds, and so on.[3–9] Credit to its ability of maintaining a stable permeation flux at high solute concentrations, MD process is often integrated with other existing separation processes for the enhancement of water recovery, reclamation of draw solution, and simultaneous production of ultrapure water.[10–12]

Among different MD configurations, direct contact MD (DCMD) is the commonest and mostly studied MD configuration. As shown in Figure 1, the heat transfer for DCMD is first transferred from the bulk feed solution to the membrane via the boundary layer and their interface. The heat is then transmitted across the membrane in both forms of latent heat and conductive heat. Subsequently, the heat is transported from the permeate interface and eventually absorbed by the cold permeate solution. Unlike DCMD, vacuum is applied in the permeate side of a vacuum MD (VMD) to induce liquid vaporization and transportation. Due to the vacuumed pores, VMD has demonstrated higher permeation fluxes and improved thermal efficiency.[13] For most VMD applications, the vaporized compounds are normally condensed by an external condenser, and additional equipment and energy costs are required to generate the vacuum conditions.[14] In recent years, via integrated design of the condensation-vacuum process, the vacuum energy consumption involved can be reduced.[15,16] These make VMD processes attractive in many applications.

Similar to other MD configurations, good wetting resistance and high permeation flux are the two main requirements for membranes fabricated for VMD processes.[17,18] However, due to the applied vacuum, membranes for VMD require stringent constraints on wetting resistance and radial-direction mechanical strength than those for DCMD. The suitable VMD membrane needs to be designed with smaller pores at the functional surface in order to generate a higher wetting resistance. In our previous report, the concept of a new generation 7-bore VMD hollow fiber was fabricated with polyvinylidene fluoride (PVDF) polymer.[19] The fabricated membrane geometry demonstrated excellent membrane wetting resistance and superior mechanical strength in both axial and radial directions. Traditional hollow fiber membranes only have one internal bore channel. The innovative hollow fiber membranes consisting of multiple bore channels generally show enhanced mechanical/chemical stability, improved long-term operation reliability, and ease of module potting.[7] In the field of filtration membranes, the commercial multibore membranes were developed by several companies or research institutes.[20,21] In our previous works, a series of multibore PVDF membranes were fabricated for DCMD and VMD processes.[19,22] In these studies, the multibore MD membranes exhibited high permeation fluxes, good energy efficiency, as well as superior stability and robustness in long-term operations. A comparison between 7-bore and

Additional Supporting Information may be found in the online version of this article.

Correspondence concerning this article should be addressed to T. S. Chung at chencts@nus.edu.sg.

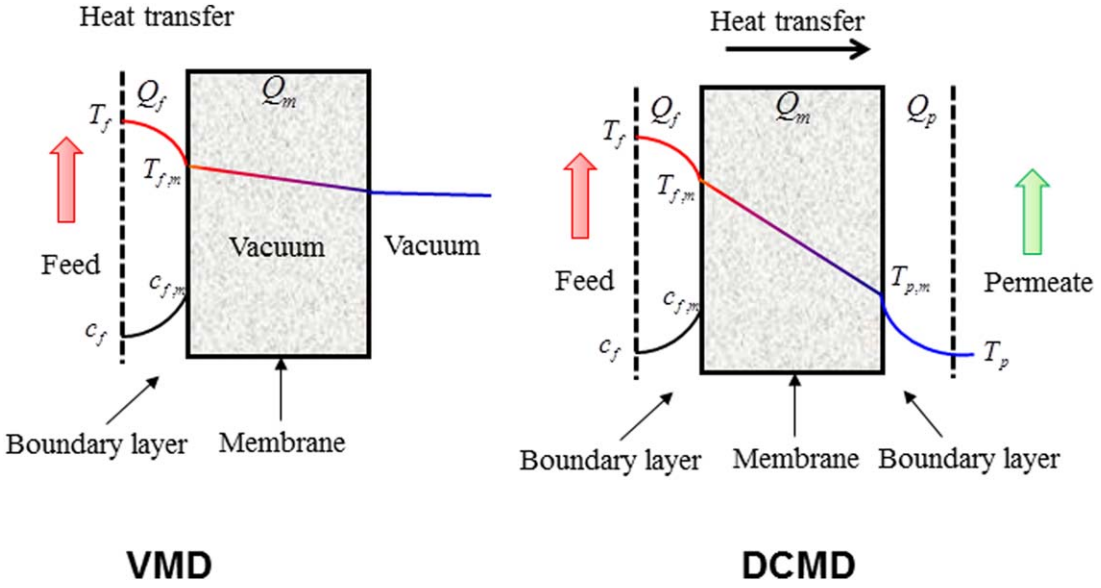

Figure 1. Heat and mass transport mechanisms of VMD (left) and DCMD (right).

[Color figure can be viewed in the online issue, which is available at wileyonlinelibrary.com.]

single-bore hollow fibers (SBF) comprising similar microstructures fabricated from alike processing parameters shows that the former has a 65% increase in antiwetting resistance.[19]

Considering the different behaviors of multibore hollow fiber (MBF) membranes in membrane formation, we aim to explore the science and optimize the fabrication parameters so that the 7-bore VMD membrane has characteristics of superior mechanical durability and wetting resistance. The fundamentals of membrane formation to relate MBF membrane morphology and VMD performance as a function of spinning conditions, such as polymer concentration, pore forming agents' chemistry and concentration as well as post-treatment methods, will be investigated in details. Various membrane properties will be characterized to study the relationship between transport mechanism and membrane microstructure. In addition to compare the performance of VMD and DCMD configurations, the effects of various VMD operational parameters and feed modes on separation performance will be investigated.

Materials and Methods

Materials

The working polymer, PVDF HSV#900 resin (specific gravity: 1.76–1.79), was purchased from Arkema. *N*-methyl-1-pyrrolidone (NMP, >99.5%), ethylene glycol (EG, >99.5%), polyethylene glycol 400 (PEG-400, >99.5%), lithium chloride (LiCl, >99.0%), and isopropanol (IPA, >99.5%) used in hollow fiber fabrication were supplied from Merck. Sodium chloride was purchased from Sigma Aldrich. The deionized water utilized in DCMD and VMD tests was produced by a Milli-Q unit (MilliPore) with a resistivity of 18 MΩ cm.

Spinneret design and membrane fabrication

The MBF PVDF membranes were fabricated via a dry-jet wet phase inversion spinning process by a specially designed spinneret consisting of seven needles. The details of spinning process and the spinneret design have been documented elsewhere.[22–24] Unlike the conventional single-bore spinneret, the 7-bore MBF spinneret had seven needles, which were distributed uniformly within the spinneret space. During spinning, the dope solution and bore fluid were extruded at specified flow rates through the spinneret by two ISCO syringe pumps (Teledyne, 1000D). The dope temperature was kept at 40°C by a thermal meter and heat jacket connected to a temperature circulator (F12, Julabo). After entering the coagulation bath, the precipitated membranes were collected by a take-up roller. To avoid the uneven distribution of polymer dope within the spinneret, the bore fluid and polymer dope were injected from the side and top of the spinneret, respectively.[25] For comparison, a traditional SBF was spun with a single-bore spinneret with the same needle dimension.

After spinning, the as-spun MBF membranes were immersed in tap water around 4 days to remove the solvent and additives. Subsequently, most of the wet fibers were frozen in a refrigerator and dried for 12 h in a freeze drier (S61-Modulyo-D, Thermo Electron). For the comparison of drying methods, three other post-treatment methods were adopted for some of the MBF membrane samples. In the air drying method, the wet fibers were hanged in an air-conditioned room under air drying for 7 days. In the IPA solvent exchange method, the membrane samples were solvent exchanged with 5 L of IPA for 3 h before air drying for 7 days. In the IPA and hexane dual-solvent exchange method, the wet membrane samples were solvent exchanged with 5 L IPA and then hexane for 3 h, respectively, before air drying for 7 days. All the spinning and post-treatment conditions have been repeated for three times to ensure the reproducibility. The detailed spinning conditions of all membranes were summarized in Table 1.

Membrane characterizations

Membrane samples were observed by an optical microscope (microscope: Olympus, SZX16; digital camera:

Table 1. Spinning Conditions of 7-Bore MBF Membranes 7bore-1 to 7bore-11

Membrane ID	7bore-1	7bore-2	7bore-3	7bore-4	7bore-5	7bore-6	7bore-7	7bore-8	7bore-9	7bore-10	7bore-11
Bore fluid			Water (0°C)					Water (0°C)			
Polymer con. (wt %)			15			**14**	**13**	**12**	14	14	14
Pore-forming agent	**EG** (10 wt %)	**PEG-400** (10 wt %)	**EG + LiCl** (9 wt % + 1 wt %)	**EG** (5 wt %)	No			EG (10 wt %)			
Dope flow rate (m min^{-1})			14					14			
Bore flow rate (m mm^{-1})			7					7			
Take up speed (m / min)			Free fall					Free fall			
External coagulant (wt %)			IPA/water: 60/40					IPA/water: 60/40			
Air gap (cm)			3					3			
Temperature (°C)			25–29					25–29			
Humidity			65%–75%					65%–75%			
Post-treatment			Freeze dry	Freeze dry	**Freeze dry**	**Freeze dry**	**IPA + hexane**[a]			**IPA**[b]	**Air dry**

[a]Solvent exchanged with IPA and hexane before air dry.
[b]Solvent exchanged with IPA.

Olympus, CMAD3), a scanning electron microscope (SEM; JEOL JSM-5600LV), and a field emission scanning electron microscope (FESEM JEOL JSM-6700F). The SEM and FESEM samples were prepared by immersing and fracturing the fiber in liquid nitrogen. Before testing, platinum was sputtered on the samples by a JEOL JFC-1100E ion sputtering device.

Porosity of hollow fiber membranes excluding bore channel space was obtained by Eq. 1[26]

$$\varepsilon = \left(1 - \frac{m_{\text{fiber}}/\rho_{\text{fiber}}}{V_{\text{fiber}} - V_{\text{channel}}}\right) \times 100\% \quad (1)$$

where V_{fiber} denotes the fiber volume, V_{channel} is the inner channel volume, m_{fiber} represents the fiber weight, and ρ_{fiber} stands for the density of the fiber material. V_{fiber} was estimated from fiber diameter and length. m_{fiber} was measured by an accurate beam balance (A&D, GR-200). ρ_{fiber} was measured by a multipycnometer (Quantachrome MVP-D160-E). For each sample, 10 measurements were carried out.

Various tensile mechanical properties (i.e., the maximum load, maximum tensile stress, maximum tensile strain, and Young's modulus) of the fibers were measured by an Instron tensiometer (Model 5542, Instron). A constant elongation rate of 10 mm min^{-1} with a starting gauge length of 50 mm was applied. For each spinning condition, 10 fiber samples were tested so as to ensure the accuracy.

The liquid entry pressure (LEP) of the fiber was tested using a home-made set-up and model seawater. More details of the set-up and operational procedures have been documented elsewhere.[19,27]

VMD desalination experiments

The VMD experiments were carried out to evaluate the permeation flux and theoretical thermal efficiency (η) of the 7-bore MBF membranes at different operation conditions. Prior to the test, the membrane modules were fabricated by assembling a predetermined number of fibers into a plastic tube of 1/2 inch outer diameter, with both ends sealed by epoxy.

Supporting Information Figure S1 shows the experimental apparatus for the characterization of VMD performance of hollow fiber membranes, where more details have been documented elsewhere.[8] Supporting Information Figure S2 illustrates two testing modes for each module during the VMD experiments; namely, (1) feed at the shell side and (2) feed at the lumen side. A model seawater containing 3.5 wt % NaCl was used as the feed.

The permeation flux for each feed temperature is calculated based on the outer surface of the membrane using Eq. 2[19]

$$N_{\text{w}} = \frac{\Delta W}{A_{\text{o}} t} \quad (2)$$

where N_{w} is the permeation flux, ΔW is the permeation weight collected over a predetermined time duration (t), and A_{o} is the effective permeation area calculated based on the outer diameter of hollow fibers.

The theoretical thermal efficiency (η) for each feed temperature is calculated using Eq. 3[27]

$$\eta = \frac{N_{\text{w}} \lambda_{\text{m}} A_{\text{o}}}{m_{\text{f}} C_{\text{p,f}} (T_{\text{l,out}} - T_{\text{l,in}})} \quad (3)$$

where λ_{m} is the latent heat of water vaporization, m_{f} is the mass flow rate of the feed solution, $C_{\text{p,f}}$ is the average

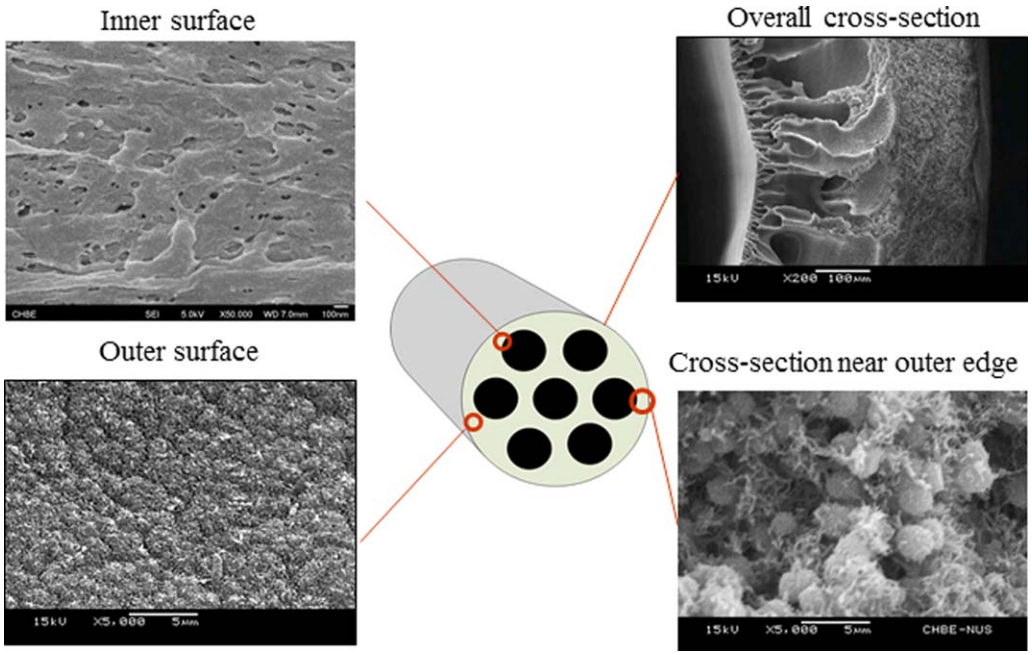

Figure 2. The cross-section and surface morphologies of a typical 7-bore MBF membrane (Membrane ID: 7bore-6).

[Color figure can be viewed in the online issue, which is available at wileyonlinelibrary.com.]

specific heat capacity of the feed solution, $T_{l,in}$ and $T_{l,out}$ are inlet and outlet temperatures of the bulk lumen and shell side solution depending on the configuration, respectively.

For comparison, the DCMD permeation flux and η value of the same selected MBF membrane were also measured using the previous set-up described in our early reports with the conditions as follows.[22,27] The inlet temperature of the feed containing 3.5 wt % NaCl was maintained at the target value by a temperature circulator (F12, Julabo), while the permeate solution was kept at 15.0°C by a cooler (RT7, Thermal Scientific). The linear velocities of feed and permeate solutions were kept at 0.3 m s^{-1}.

Results and Discussion

General membrane characterizations

Figure 2 displays the membrane surface and cross-section morphologies of a typical MBF membrane with an ID of 7bore-6. As designed, the membrane consists of seven uniformly distributed inner bore channels. Because a strong bore fluid at the reduced temperature (i.e., water at 0°C) is used, the PVDF nucleation and crystallization is suppressed. This results in an inner surface with smaller pores but high surface porosity. Conversely, a weak external coagulant (i.e., 60/40 IPA/water) induces a delayed demixing that facilitates pore formation and PVDF crystallization at the region close to the outer surface.[19,27] Hence, the outer surface and the outer cross-section area show a porous structure with interconnected globules. The micromorphology and macrogeometry coincide with the proposed requirements of a VMD MBF membrane.

Exploration of pore forming agents

To obtain a PVDF membrane with a desirable porous morphology and permeation performance, the addition of pore forming agents into polymer dopes is an effective and widely used method.[28,29] The pore forming agents that have been used in PVDF membrane fabrication include small molecule nonsolvents (i.e., EG, alcohol, and water), inorganic salts (i.e., LiCl and $CaCl_2$), and macromolecular polymer additives [i.e., PEG and polyvinylpyrrolidone (PVP)].[14,30–32] Their physicochemical properties play an important role in membrane formation and membrane separation performance. For example, if a high molecular weight PEG or PVP is used, a decrease in membrane hydrophobicity or even a conversion from hydrophobicity to hydrophilicity is often observed due to the residue of the hydrophilic PEG or PVP polymer within the membrane matrix. In this work, three types of pore forming agents have been investigated. Figure 3 shows the cross-section and surface morphologies of MBF membranes fabricated from dopes comprising: (1) 7bore-1–10 wt % EG, (2) 7bore-2–10 wt % PEG-400, and (3) 7bore-3–9 wt % EG + 1 wt % LiCl. Figure 4 displays various membrane properties, such as porosity, maximum load, contact angle, and VMD flux, as a function of different pore forming agents used.

EG and PEG are nontoxic pore forming agents (hazardous in case of ingestion).[27,33] They have been widely used in membrane manufacture to generate pores and porosity for flux enhancement.[27] As a nonsolvent in the PVDF-NMP binary system, the addition of EG and PEG not only increases dope viscosity but also brings solutions closer to gelation points. As a result, membranes spun from dopes containing EG and PEG would have a more porous structure at membrane cross-section and surfaces. Due to their differences in nonsolvent strength and molecular size, the membrane fabricated with PEG-400 has bigger macrovoids at the cross-section than the one with EG. Similar observations were found in the case when alcohol and water were used as pore forming agents.[34] Due to the bigger macrovoids, the MBF membrane spun with PEG-400 exhibits enhanced permeation fluxes but reduced mechanical strength. Unlike some cases where higher molecular weight PEG, polyethylene-oxide (PEO), and PVP are used, the contact angle of the current fiber is not much affected by the addition of PEG-400 into the polymer dope. This indicates an almost complete removal of small PEG-400 molecules from the nascent membranes because PEG-400 is small and highly soluble in water.

LiCl is an inorganic pore forming agent during membrane preparation.[32] The macromolecular complex formed between

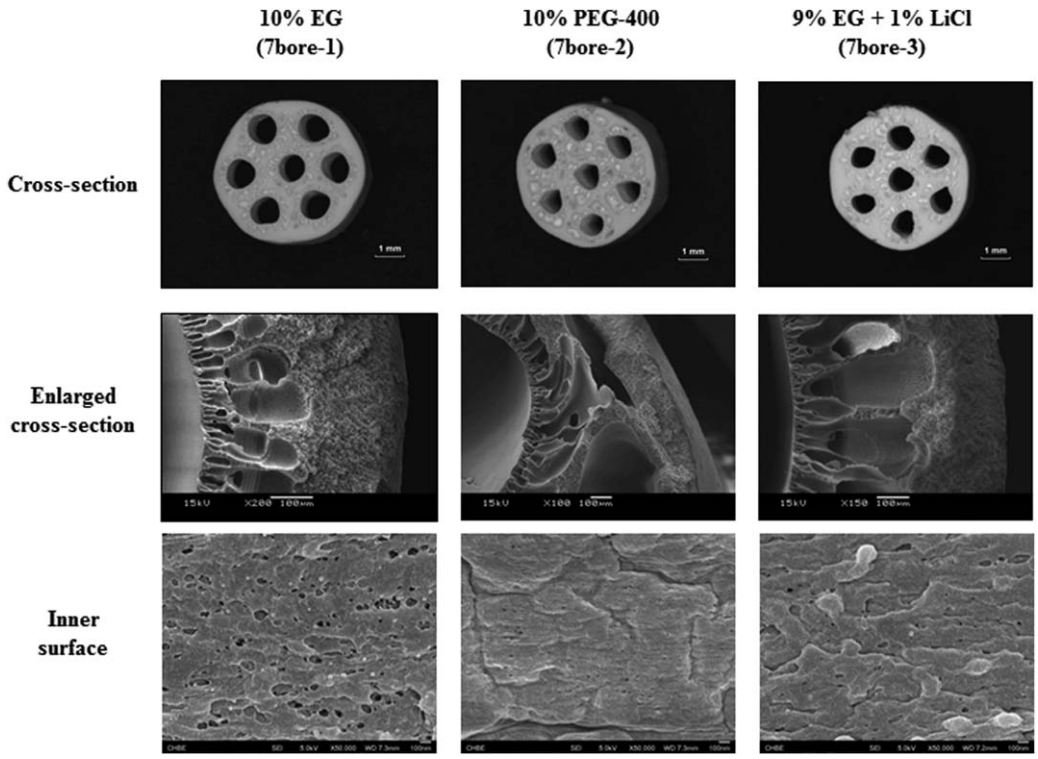

Figure 3. The cross-section and surface morphologies of 7-bore MBF membranes spun from dopes containing different pore-forming agents.

Li^+ and electron donating groups of many solvents (i.e., NMP) could increase dope viscosity and enhance permeation flux.[35] However, a severe reduction in mechanical strength is observed in the case of PVDF membranes. Hence, a combination of 9 wt % EG + 1 wt % LiCl is used in an attempt to balance the membrane mechanical strength and permeation

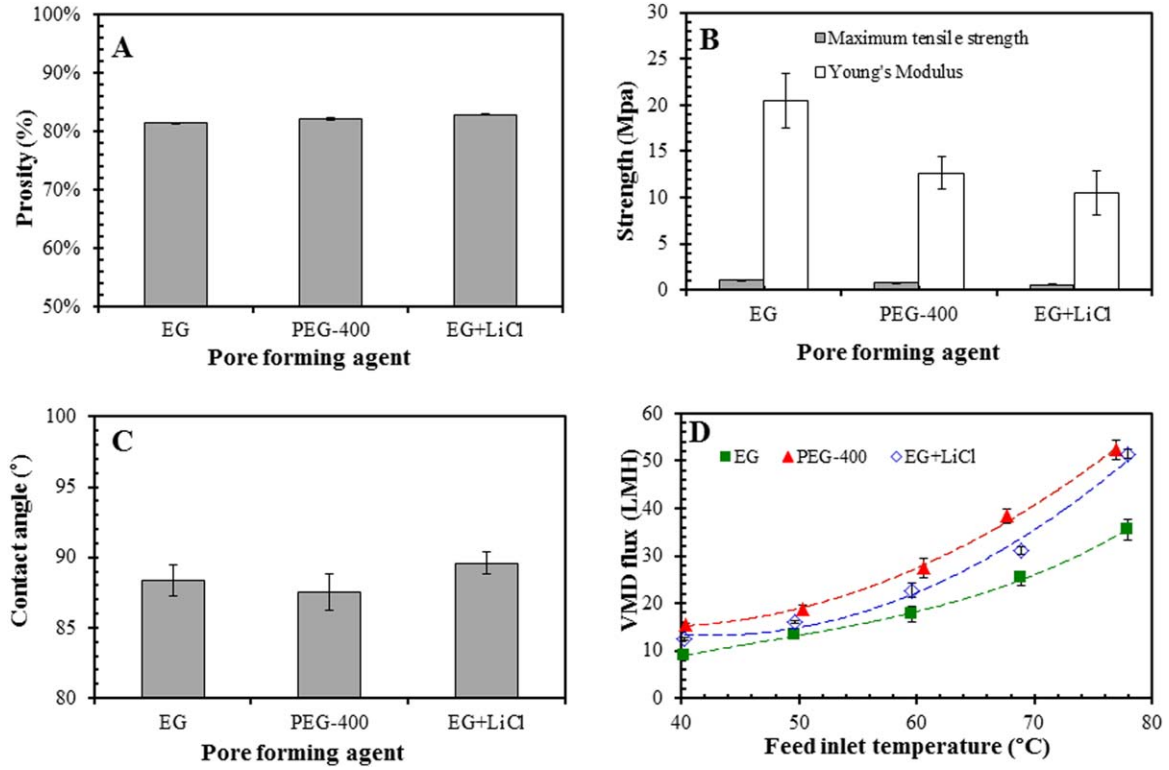

Figure 4. (A) Bulk porosity, (B) mechanical strength, (C) contact angle and (D) VMD permeation flux of 7-bore MBF membranes spun from dopes containing different pore-forming agents.

[Color figure can be viewed in the online issue, which is available at wileyonlinelibrary.com.]

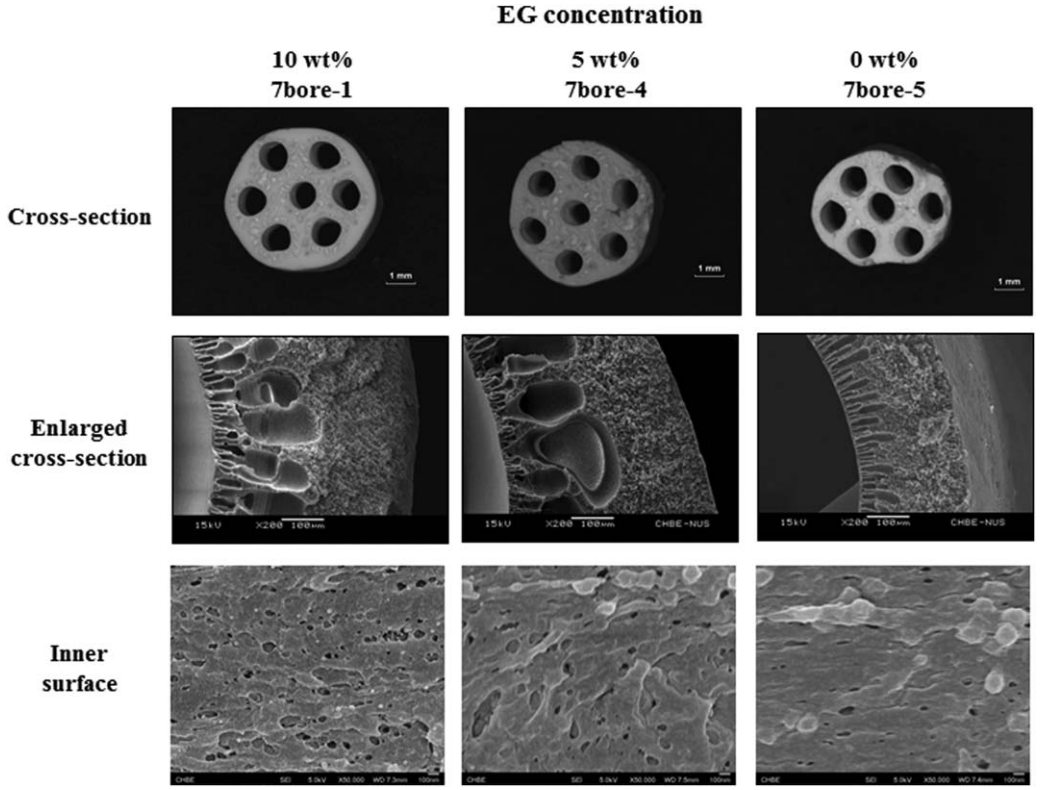

Figure 5. The cross-section and inner surface morphologies of 7-bore MBF membranes spun from dopes with different EG concentrations.

properties. As compared with the membrane fabricated with EG only, there is an increase in maximum tensile strain from 29.6 to 35.2%, but a decrease in Young's Modulus from 20.47 to 10.5 MPa. This is probably caused by the Li^+-PVDF macromolecular complex which generates a different globule microstructure in the membrane matrix. Supporting Information Figure S3 shows the cross-section microstructures taken at the middle of the membrane walls (the same position). The membranes fabricated with EG and PEG-400 additives consist of interconnected globule structures, whereas the membrane fabricated with EG+LiCl additives shows only small globules. Proven by previous reports, this kind of globule structure without any interconnection often suffers from a poor mechanical strength.[36–38] Owing to the lower mass transport resistance of globule structure and larger macrovoids, the VMD permeation flux of this MBF membranes is higher than that of the MBF fabricated with EG only. However, occasional increase of permeate salinity is noticed during the repeated VMD performance tests. Hence, the combined EG-LiCl pore forming agent is still not preferred in this application.

Effects of nonsolvent concentration

With a solubility parameter of 36.2 MPa, the coagulation strength of EG is between water (47.8 MPa) and IPA (23.5 MPa).[4,39] Figure 5 shows the cross-section and surface morphologies of MBF membranes fabricated from dopes comprising various EG from 0 to 10 wt %. The MBF membranes spun from dopes containing 5 and 10 wt % EG are more porous in both cross-section and surfaces, while no many surface pores can be observed for the membrane spun without EG. Although all membranes have finger-like macrovoids, the membrane spun without EG shows much smaller macrovoid sizes due to the hydrophobic nature of PVDF and less water intrusion. These morphological findings agree well with previous reports on the effects of nonsolvent pore forming agents for PVDF membranes.[4,39,40] Figure 6 displays various membrane properties, such as porosity, maximum load, LEP, burst pressure, and VMD flux as a function of EG content for these MBF membranes. When the dope does not contain EG, the resultant membrane exhibits the lowest bulk porosity of 66.8%. With increasing EG content, porosity increases up to 81.3%, VMD flux also increases, whereas Young's modulus, LEP, and burst pressure drops.

Effects of polymer concentration

Figure 7 illustrates the SEM images of cross-section and surface morphologies of MBF membranes fabricated from dopes with different PVDF concentrations from 12 to 15 wt %. Water at 0°C was used as the bore fluid for all membranes. Regardless of which polymer concentration, all hollow fiber membranes have finger-like macrovoids located immediately underneath the inner surface. However, due to the low dope viscosity at a low polymer concentration (i.e., 12 wt %), water intrusion is severe for fibers spun from a low polymer concentration. The resultant membrane has finger-like macrovoids almost across the entire membrane thickness. In addition, its outer surface shows a high percentage of polymer-lean regions magnified by large surface pores and a diverse pore size distribution.[41] As polymer concentration increases, water intrusion is suppressed and there are more regions of sponge-like structure near the outer surface. Figure 8 displays various membrane properties as a function of PVDF concentration in spinning dopes. The MBF membranes spun from lower polymer concentrations show higher porosity, reduced mechanical strength, lower LEP, and burst

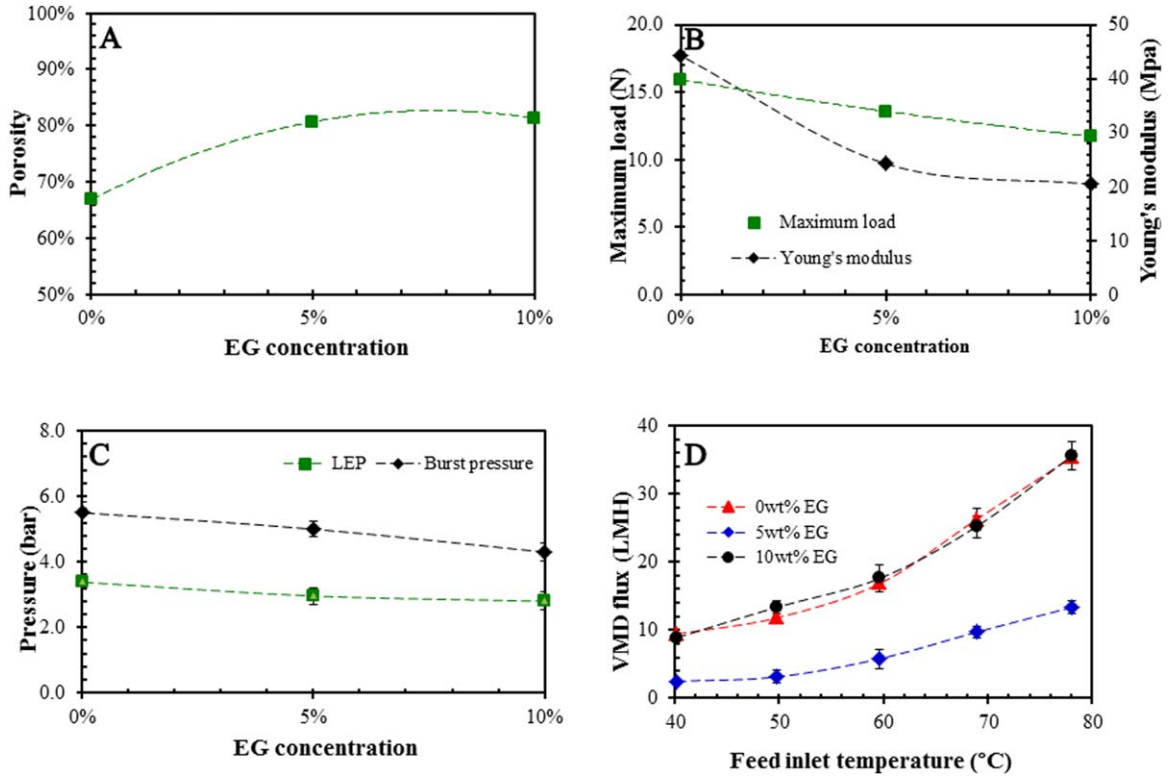

Figure 6. (A) Bulk porosity, (B) mechanical strength, (C) LEP and burst pressure, and (D) VMD permeation flux with 7-bore MBF membranes fabricated from different EG concentrations.

[Color figure can be viewed in the online issue, which is available at wileyonlinelibrary.com.]

pressure. Correspondingly, these membranes not only have larger surface pores and higher porosity but also exhibit impressive permeation fluxes for all feed temperatures. For instance, at a feed temperature of 80°C, the VMD flux of the MBF membrane spun from 12 wt % PVDF is as high as 72 L m^{-2} h^{-1} (LMH). However, although no leakage was found during the VMD experiment of this MBF membrane, its lower LEP (1.3 bar) might be an issue during the long-term VMD operation if the vacuum level is high.

Effects of post-treatments for drying

Unlike reverse osmosis (RO), micro-filtration (MF), and most membranes used for liquid separation, MD membranes need to be thoroughly dried after membrane fabrication.

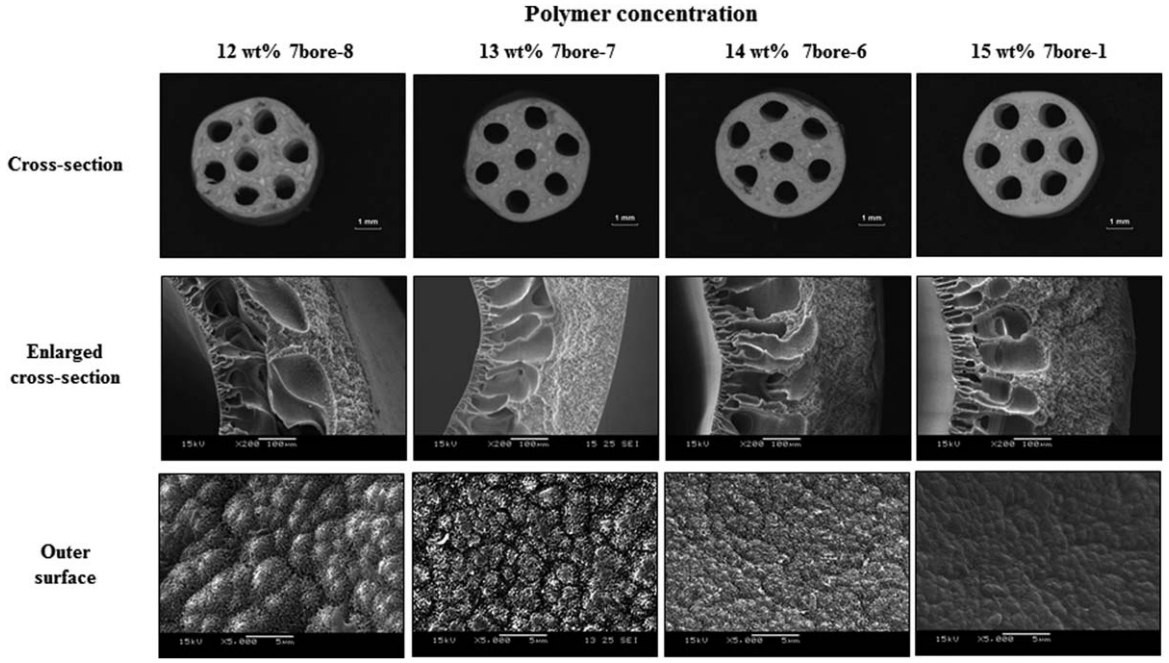

Figure 7. The cross-section and inner surface morphologies of 7-bore MBF membranes spun from different dope concentrations.

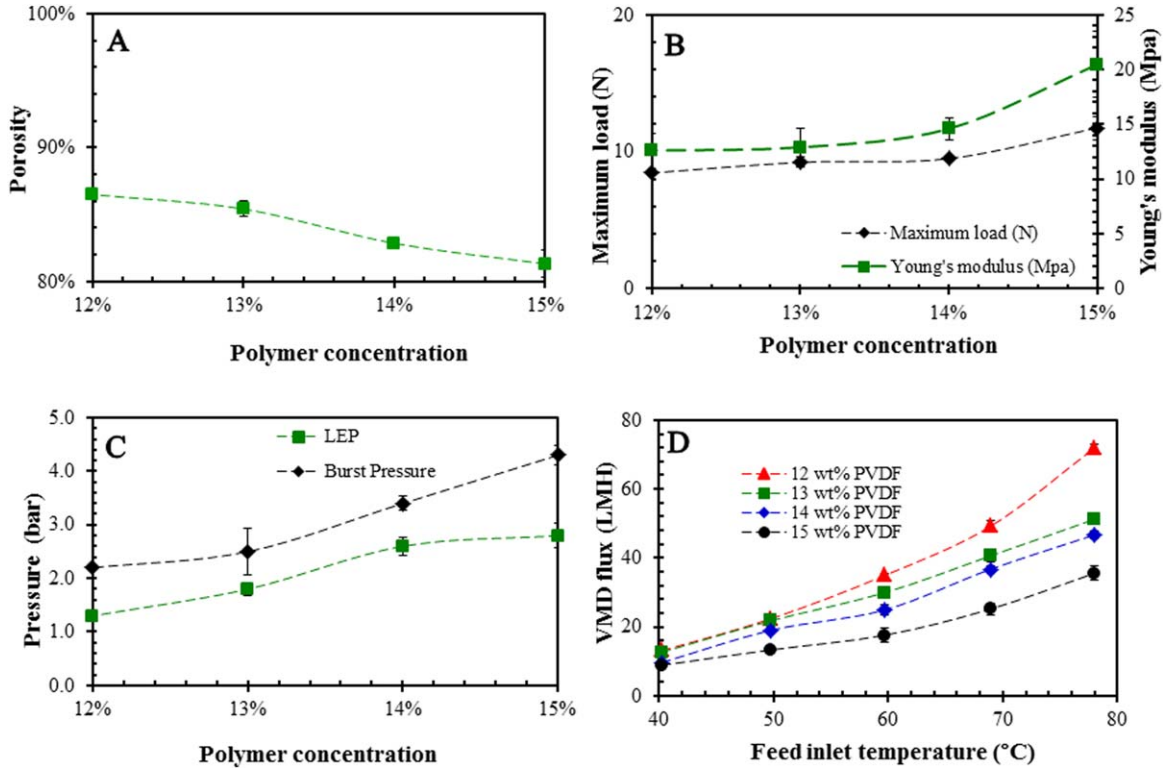

Figure 8. (A) Bulk porosity, (B) mechanical strength, (C) LEP and burst pressure, and (D) VMD permeation flux with 7-bore MBF membranes fabricated from different polymer concentrations.

[Color figure can be viewed in the online issue, which is available at wileyonlinelibrary.com.]

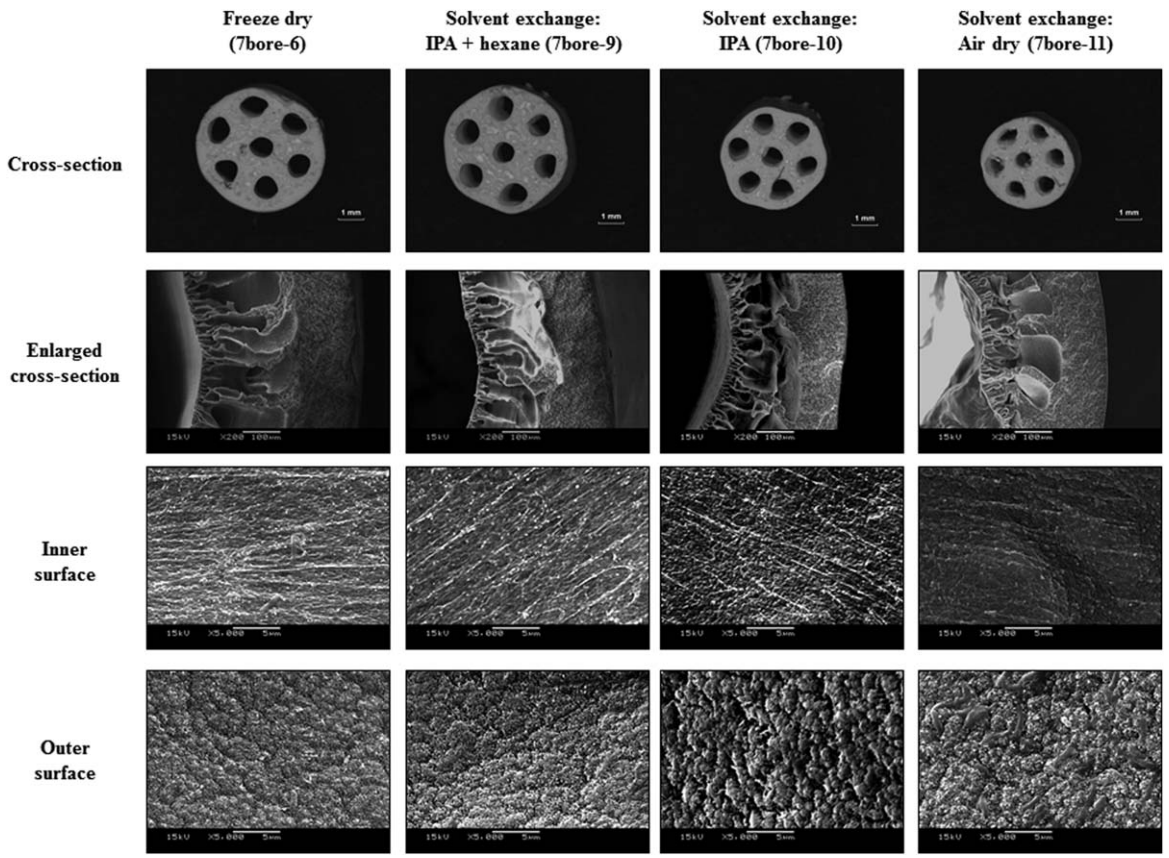

Figure 9. The cross-section and surface morphologies of 7-bore MBF membranes with different post-treatments.

Table 2. Characteristic Properties of 7-Bore MBF Membranes 7bore-1 to 7bore-11

Membrane ID	7bore-1	7bore-2	7bore-3	7bore-4	7bore-5	7bore-6	7bore-7	7bore-8	7bore-9	7bore-10	7bore-11
OD/ID (μm / μm)	5622/1199	5102/934	5053/929	5450/1033	4882/1139	5344/1074	5389/1017	5349/1054	5618/1083	4452/961	4079/820
Porosity (%)	81.3 ± 0.1	82.9 ± 0.1	82.1 ± 0.1	80.7 ± 0.1	66.8 ± 0.2	82.8 ± 0.1	85.4 ± 0.2	86.5 ± 0.1	82.8 ± 0.2	69.1 ± 0.1	55.3 ± 0.3
Maximu load (N)	11.74 ± 0.85	10.58 ± 0.47	10.33 ± 0.42	13.58 ± 0.54	15.95 ± 0.23	9.49 ± 0.15	9.22 ± 0.37	8.44 ± 0.15	10.33 ± 0.42	13.69 ± 0.46	28.25 ± 0.38
Maximum tensile stress (MPa)	1.03 ± 0.05	0.74 ± 0.03	0.584 ± 0.02	0.94 ± 0.04	1.59 ± 0.02	0.67 ± 0.01	0.66 ± 0.03	0.59 ± 0.04	0.72 ± 0.03	1.5 ± 0.05	3.71 ± 0.05
Young's modulus (MPa)	20.47 ± 3.0	12.6 ± 1.76	10.5 ± 2.41	21.26 ± 3.18	44.3 ± 6.7	12.9 ± 1.0	12.8 ± 1.7	12.6 ± 1.6	17.9 ± 0.85	38.3 ± 7.11	148.4 ±15.3
Maximum tensile strain (%)	29.6 ± 5.1	26.6 ± 5.24	35.2 ± 2.26	17.4 ± 2.0	23.5 ± 1.2	31.8 ± 2.6	29.0 ± 3.8	30.5 ± 3.7	33.4 ± 3.5	23.9 ± 1.3	6.3 ± 1.6
LEP (bar)	2.66 ± 0.14	–	–	2.26 ± 0.25	2.38 ± 0.19	2.60 ± 0.17	1.86 ± 0.13	1.28 ± 0.10	2.67 ± 0.09	4.75 ± 0.37	3.89 ± 0.25
Burst Pressure (bar)	4.28 ± 0.27	–	–	5.08 ± 0.23	5.57 ± 0.31	3.41 ± 0.24	2.47 ± 0.43	2.31 ± 0.35	3.38 ± 0.31	6.21 ± 0.63	11.41 ±3.14

However, the drying of wet MD membranes at ambient temperatures results in a severe membrane shrinkage and reduction in permeation performance.[40,42] The effect that takes place during membrane drying is attributed to the capillary force acting on the fine pores. Due to the high surface tension, the force at the air-water interface is so large that the pore walls are pulled together and collapsed.[43] The structural collapse has greatly restricted water flux across the membrane. Although commonly used freeze dry has been proven to be an effective post-treatment method to maintain the pore structure, its real application may be constrained by the treatment capacity and energy consumption.[27] Hence, different solvent exchange treatments followed by air dry have been evaluated in this work. Similar to the post-treatment of gas separation membranes, the water-filled MBF MD membranes are first immersed in water soluble IPA, after which the IPA is replaced by hexane, which is a highly volatile alcohol soluble organic compound.[44,45] During the two-step solvent exchange process, the membrane color changes noticeably from white to semitransparent and then back to white, indicating a complete removal of water and IPA.

Four different post-treatments are evaluated; namely, (1) 7bore-6—freeze dry, (2) 7bore-9—IPA followed by hexane and air dry, (3) 7bore-10—IPA followed by air dry, and (4) 7bore-11—air dry. For easy comparison, these four MBF membranes were spun from the same dope under the same conditions, as shown in Table 1. Figure 9 displays their cross-section and surface morphologies after different post-treatments, whereas Table 2 and Figure 10 compare their physiochemical properties and VMD performance. Comparing with the membrane post-treated by freeze dry, the membranes post-treated by IPA or water and then air dry have higher shrinkages. As IPA has lower hydrogen bonding and surface tension than water,[46] the IPA-treated membrane (7bore-10) has higher porosity, larger pore size, and larger membrane dimension than the directly air dried membrane (7bore-11). In addition, the shrinkage does not only take place on the outer surface, but also on the inner surface. However, the reduction in the inner diameter is much smaller than the outer diameter. Besides, bulk densification and pore shrinkage can be noticed. As a result, the 7bore-10 and 7bore-11 have much higher LEP values and burst pressures but much lower VMD permeation fluxes due to the reduced pore sizes and bulk porosity.[47] Although their LEP and burst pressures far exceed the requirements for VMD operations, their fluxes are not impressive. Thus, they are not preferred for VMD applications.

Interestingly, there are no sharp differences in morphologies and bulk porosity between membranes treated by freeze dry and two-step solvent exchange (i.e., IPA + hexane) followed by air dry except the VMD flux is slightly lower for the membrane after two-step solvent exchange. The well maintained microstructure indicates the minimum pore collapse during freeze dry and hexane evaporation. Clearly, the low surface tension of volatile hexane contributes to the integrity of pore structure due to the low capillary force between liquid hexane and pore walls.[44] It is interesting to note that the mechanical strength and burst pressure of the membrane post-treated by the two-step solvent exchange are slightly higher than that post-treated by freeze dry. This may be attributed to minor damages in membrane microstructure during freeze dry. As there is a 10% decrease in water density from liquid to ice, the

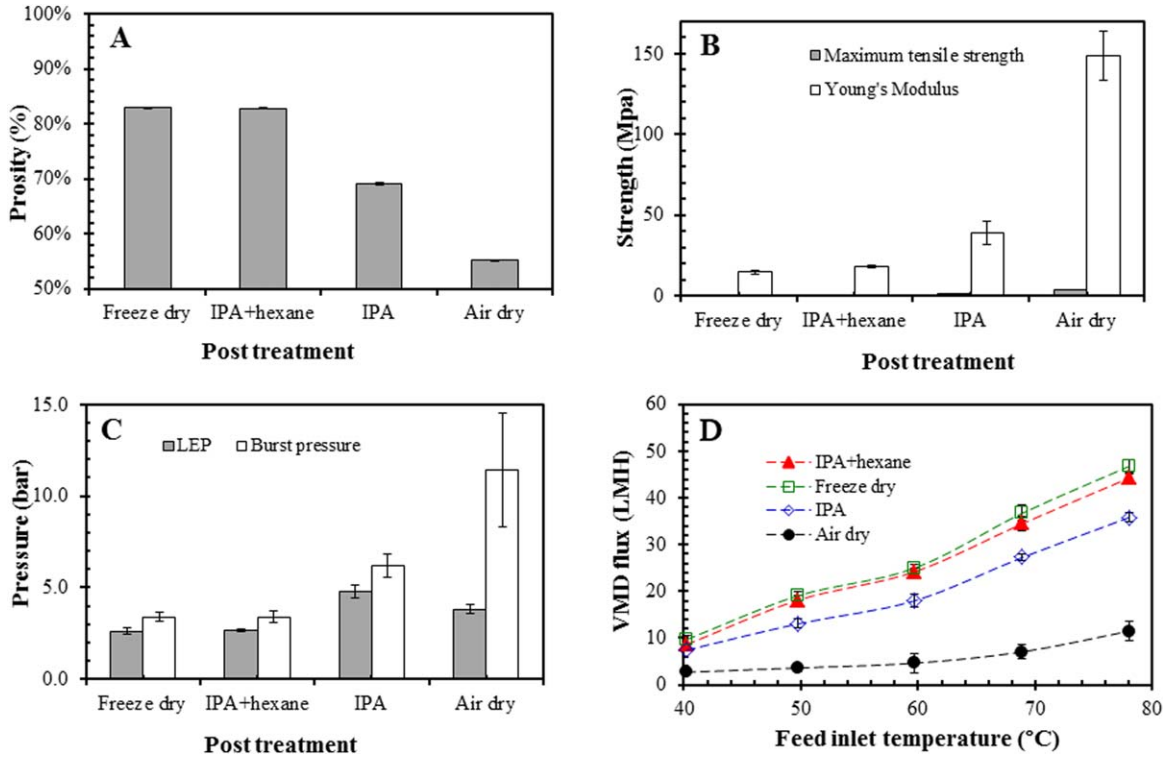

Figure 10. (A) Bulk porosity, (B) mechanical strength, (C) LEP and burst pressure, and (D) VMD permeation flux of 7-bore MBF membranes after different post-treatment methods and then air dry.

[Color figure can be viewed in the online issue, which is available at wileyonlinelibrary.com.]

expansion of water volume during freeze dry may deform membrane microstructure. From this aspect, the solvent exchange method consisting of IPA and then hexane may be a better choice.

Investigations on the VMD and DCMD performance

Comparison with DCMD Performance. Figure 11A displays a comparison of permeation flux as a function of feed temperature using the membrane with ID 7bore-1 for both VMD and DCMD processes. The permeation fluxes of both MD configurations increase nonlinearly with the feed inlet temperature. This agrees well with previous studies on MD processes.[35,48,49] Consistent with the hypotheses in the Introduction section, the VMD configuration has a higher permeation flux than the DCMD owing to the vacuumed pores and the better thermal insulation. The vacuum applied in MD not only generates the significant Poiseuille flow, but also minimizes the thermal conductivity and temperature polarization effect, thus simultaneously increases the effective driving force across the membrane. As a consequence, the flux is greatly enhanced.[48,49]

There are different diffusion mechanisms during VMD and DCMD processes even for the same membrane. The transport mechanism of water vapor in the pores of MD membranes is generally determined by the relative size of pore diameter and the mean free path (λ) of water vapor and air. As air and vapor are continuously removed from the membrane pores in VMD, the molecular collision and consequently, molecular diffusion are dramatically reduced under high vacuum. The mean free path of water vapor and air mixture can be mathematically expressed as Eq. 4[50]

$$\lambda = \frac{k_B T_m}{\pi\left(\frac{\sigma_w+\sigma_a}{2}\right)P_T}\frac{1}{\sqrt{1+\left(\frac{M_w}{M_a}\right)}} \quad (4)$$

where λ is the mean molecular free path evaluated at the average membrane temperature (T_m) and pressure (P_T); k_B is the Boltzmann constant; σ_w and σ_a are the collision diameters of water and air molecules, respectively; M_w and M_a are the molecular weights of water and air, respectively.

This equation implies that λ has a reverse relationship with the total pressure (vapor density) of the mixture. Assuming the pressure in membrane pores is maintained at 10 mbar, the mean free path in the VMD process at 50°C is around 11.1 μm, whereas it is about 0.11 μm in a DCMD process operated at an atmospheric pressure. As the pore size of the MBF is around 0.1 μm, the diffusion of water vapor is dominated by paralleled Knudsen diffusion and Poiseuille flow in the VMD process, whereas Knudsen and molecular diffusion in series are dominant in the DCMD process. As a result, the overall resistance for vapor diffusion in a VMD process is lower than the DCMD process.

Figure 11B compares the η values of VMD and DCMD processes as a function of feed inlet temperature. η is defined as the ratio of the latent heat flux to the total heat transfer (i.e., the sum of latent and conductive heat fluxes). It has been widely used as an indication of thermal efficiency for MD.[51] Owing to the nonlinear and linear relationship of these two heat fluxes with the feed temperature, η often increases with an increase in feed temperature.[52] Interestingly, much higher values are obtained for VMD, especially in the lower feed temperature region. As compared with DCMD, η of VMD is insensitive with feed temperature. When the feed temperature increases from 40 to 80°C, η

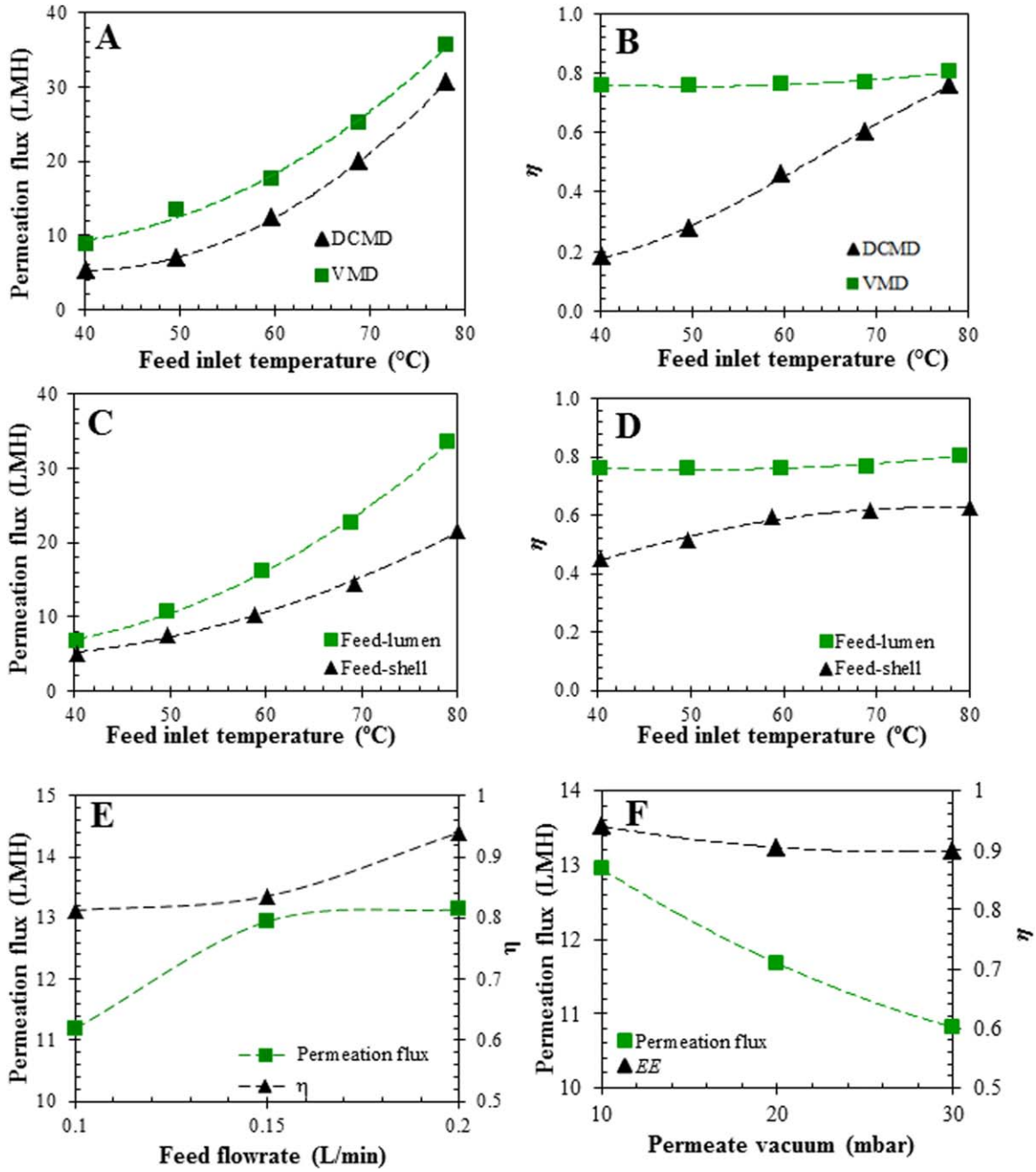

Figure 11. Comparison of (A) permeation flux and (B) η values of 7bore-1 between VMD and DCMD processes.

(VMD operation conditions: feed velocity: 0.15 L/min, permeate vacuum: 10 mbar. DCMD operation conditions: feed flow rate: 0.15 L/min, permeate flow rate: 0.15 L/min, permeate inlet temperature: 15°C). (C) VMD permeation flux and (D) η of 7bore-1 with different flow configurations. Feed linear velocity: 0.25 m/s; permeate side vacuum level: 10 mbar. VMD permeation flux and η of 7bore-1 with different feed flow rates and permeate side vacuum. (E) Feed inlet temperature: 50°C, permeate vacuum level: 10 mbar; (F) feed inlet temperature: 50°C, feed flow rate: 0.15 L/min. All conditions were tested under feed at lumen side mode. [Color figure can be viewed in the online issue, which is available at wileyonlinelibrary.com.]

increases from 20 to 76% for DCMD, whereas it only varies from 76 to 78% for VMD. The high η value and its insensitivity to feed temperature demonstrate the superiority and diversity of VMD over DCMD in real industrial applications.

VMD Performance with Different Feed Modes. There are two feed modes for a hollow fiber module; namely, (1) feed at the lumen side and (2) feed at the shell side. Figures 11C, D compares the effects of feed mode and temperature on η value and VMD flux using the outer surface areas for flux calculations. Interestingly, the mode of feed at the lumen side gives higher fluxes and higher η values than the mode of feed at the shell side for all temperatures. This enhanced flux for the feed at lumen side is a unique feature of the multibore configuration because previous VMD reports using SBFs show contradictory results.[53,54] This arises from the fact that MBF and SBF membranes display different VMD performance characteristics. Under the mode of feed at the lumen side, the MBF membrane not only provides a much higher effective evaporation surface (i.e., 48% higher for 7bore-1) but also better thermal insulation than the SBF membrane. Though all fibers are properly sealed

with the thermal insulation foam, heat is continuously releasing from the hot feed to the surroundings. As the mode of feed at the lumen side has a less heat loss to the surroundings than the other mode, it is preferable for the MBF-based VMD process.

VMD Performance with Different Operational Parameters. Figures 11E, F show the VMD permeation flux as functions of feed flow rate and vacuum pressure, respectively. All the tests are under feed at lumen side mode. Both VMD flux and η increase with feed flow rate due to the higher convective heat transfer coefficient and lower temperature polarization. These findings are consistent with the previous reports on all MD configurations.[10,27,40] In other words, an increase in feed flow rate promotes the turbulence flow at the boundary layer and enhances the efficiency of convective heat transfer. As a result, the loss of driving force at the boundary layer region is reduced, whereas the effective driving force at membrane surface is increased.

As demonstrated in Figure 11F, an increase in pressure in the permeate side results in a decrease in both flux and η values. The flux decreases from 13 to 11 LMH, and the η drops from 94 to 90% when the permeate side pressure increases from 10 to 30 mbar. The reduced permeation flux is mainly caused by the reduction of driving force for vapor diffusion. The vapor pressure of 3.5 wt % NaCl solution is around 121 mbar.[6,27] As an approximation without considering the boundary layer effect, the vapor pressure of the 3.5 wt % NaCl solution decreases from around 111 to 91 mbar when the permeate side pressure increases from 10 to 30 mbar. This vapor pressure reduction agrees well with the decline of VMD fluxes.

Conclusions

In this work, we have conducted hollow fiber spinning engineering to tailor the morphologies of multibore PVDF hollow fiber membranes for the VMD application. The desired VMD membrane morphology with a tight contact surface pore and porous cross-section can be fabricated with a combination of a strong bore fluid, a high content of pore forming agent, a suitable polymer concentration in the dope and two-step solvent exchange drying. A higher concentration of powerful pore forming agent EG is desired to generate pores at both membrane cross-section and surfaces. A lower PVDF concentration generates larger pores and higher porosity. Among four types of membrane post-treatments, two-step solvent exchange (IPA, hexane) followed by air drying could maintain pore structure and minimize membrane shrinkage to ensure high VMD performance.

Compared with the DCMD configuration, the VMD performance of the same membrane exhibits a much higher permeation flux and theoretical thermal efficiency. In addition, the theoretical thermal efficiency of DCMD increases almost linearly with feed inlet temperature, whereas that of VMD shows almost no effect. The MBF membrane exhibits a better VMD flux and theoretical thermal efficiency under the operation mode of feed at the lumen side due to a larger effective surface area and a reduced thermal loss to the surrounding. A better VMD flux and thermal efficiency can also be obtained with a higher feed flow rate and/or a lower permeate pressure.

Acknowledgments

This research was funded by the Singapore National Research Foundation under its Competitive Research Program for the project entitled, "Advanced FO Membranes and Membrane Systems for Wastewater Treatment, Water Reuse, and Seawater Desalination" (grant number: R-279-000-339-281). The authors also appreciate Dr. Y. K. Ong, Dr. K. Y. Wang, and Dr. R. C. Ong for their valuable suggestions and comments.

Literature Cited

1. Curcio E, Drioli E. Membrane distillation and related operations—a review. *Sep Purif Rev*. 2005;34(1):35–86.
2. Escobar IC. Membrane developed systems for water and wastewater treatment. *Environ Prog*. 2005;24(4):355–357.
3. Maab H, Francis L, Al-saadi A, Aubry C, Ghaffour N, Amy G, Nunes SP. Synthesis and fabrication of nanostructured hydrophobic polyazole membranes for low-energy water recovery. *J Membr Sci*. 2012;423–424:11–19.
4. Khayet M, Velázquez A, Mengual JI. Direct contact membrane distillation of humic acid solutions. *J Membr Sci*. 2004;240(1–2):123–128.
5. Belafi-Bako K, Koroknai. Enhanced water flux in fruit juice concentration: Coupled operation of osmotic evaporation and membrane distillation. *J. Membr Sci*. 2006;269(11–12):187–193.
6. Tomaszewska M, Gryta M, Morawski AW. Study on the concentration of acids by membrane distillation. *J Membr Sci*. 1995;102(1–3):113–122.
7. Song L, Ma Z, Liao X, Kosaraju PB, Irish JR, Sirkar KK. Pilot plant studies of novel membranes and devices for direct contact membrane distillation-based desalination. *J Membr Sci*. 2008;323(2):257–270.
8. Khayet M, Mengual JI, Matsuura T. Porous hydrophobic/hydrophilic composite membranes: application in desalination using direct contact membrane distillation. *J Membr Sci*. 2005;252(1–2):101–113.
9. Criscuoli A, Bafaro P, Drioli E. Vacuum membrane distillation for purifying waters containing arsenic. *Desalination*. 2012;323:17–21.
10. Ge Q, Wang P, Wan C, Chung TS. Polyelectrolyte-promoted forward osmosis-membrane distillation (FO-MD) hybrid process for dye wastewater treatment. *Environ Sci Technol*. 2012;46(11):6236–6243.
11. Wang P, Chung TS. A conceptual demonstration of freeze desalination-membrane distillation (FD-MD) hybrid desalination process utilizing liquefied natural gas (LNG) cold energy. *Water Res*. 2012;46(13):4037–4052.
12. Phattaranawik J, Fane AG, Pasquier ACS, Bing W, Wong FS. Experimental study and design of a submerged membrane distillation bioreactor. *Chem Eng Technol*. 2009;32(1):38–44.
13. Li B, Sirkar KK. Novel membrane and device for vacuum membrane distillation-based desalination process. *J Membr Sci*. 2005;257(1–2):60–75.
14. Simone S, Figoli A, Criscuoli A, Carnevale MC, Rosselli A, Drioli E. Preparation of hollow fibre membranes from PVDF/PVP blends and their application in VMD. *J Membr Sci*. 2010;364(1–2):219–232.
15. Mericq J-P, Laborie S, Cabassud C. Evaluation of systems coupling vacuum membrane distillation and solar energy for seawater desalination. *Chem Eng J*. 2011;166(2):596–606.
16. Xu Y, Zhu B-k, Xu Y-y. Pilot test of vacuum membrane distillation for seawater desalination on a ship. *Desalination*. 2006;189(1–3):165–169.
17. Gryta M, Tomaszewska M. Heat transport in the membrane distillation process. *J Membr Sci*. 1998;144(1–2):211–222.
18. Gryta M, Tomaszewska M, Morawski AW. Membrane distillation with laminar flow. *Sep Purif Technol*. 1997;11(2):93–101.
19. Wang P, Chung TS. A new generation asymetric multi-bore hollow fiber membrane for sustainable water production via vacuum membrane distillation. *Environ Sci Technol*. 2013;47(12):6272–6278.
20. R&D: Ongoing development of our Multibore® membranes. http://www.inge.ag/assets/inge_nl_en_11.pdf. Published January 21, 2013. Accessed December 13, 2013.
21. Kristal®-The ultrafiltration advatages. http://www.hyfluxmembranes.com/pdf/brochures/Kristal.pdf. Accessed December 13, 2013.
22. Wang P, Chung TS. Design and fabrication of lotus-root-like multibore hollow fiber membrane for direct contact membrane distillation. *J Membr Sci*. 2012;421–422:361–374.
23. Su J, Ong RC, Wang P, Chung TS, Helmer BJ, de Wit JS. Advanced FO membranes from newly synthesized CAP polymer for

wastewater reclamation through an integrated FO-MD hybrid system. *AIChE J*. 2012;59:1245–1254.
24. Jiang LY, Chung TS, Kulprathipanja S. Fabrication of mixed matrix hollow fibers with intimate polymer-zeolite interface for gas separation. *AIChE J*. 2006;52(8):2898–2908.
25. Tung KL, Li YL, Hu CC, Chen YS. Power-law polymer solution flow in a converging annular spinneret: analytical approximation and numerical computation. *AIChE J*. 2012;58(1):122–131.
26. Song ZW, Jiang LY. Optimization of morphology and performance of PVDF hollow fiber for direct contact membrane distillation using experimental design. *Chem Eng Sci*. 2013;201:130–143.
27. Wang P, Teoh MM, Chung TS. Morphological architecture of dual-layer hollow fiber for membrane distillation with higher desalination performance. *Water Res*. 2011;45(17):5489–5500.
28. Sukitpaneenit P, Chung TS. Molecular design of the morphology and pore size of PVDF hollow fiber membranes for ethanol-water separation employing the modified pore-flow concept. *J Membr Sci*. 2011;374(1–2):67–82.
29. Zhang M, Zhang L, Cheng LH, Zhang L, Cheng L, Xua K, Xu Q, Chen H, Lai J, Tung K. Extracorporeal endotoxin removal by novel l-serine grafted PVDF membrane modules. *J Membr Sci*. 2012;405–406:104–112.
30. Khayet M, Feng CY, Khulbe KC, Matsuura T. Study on the effect of a non-solvent additive on the morphology and performance of ultrafiltration hollow-fiber membranes. *Desalination*. 2002;148(1–3):321–327.
31. Fontananova E, Jansen JC, Cristiano A, Curcio E, Drioli E. Effect of additives in the casting solution on the formation of PVDF membranes. *Desalination*. 2006;192(1–3):190–197.
32. Tomaszewska M. Preparation and properties of flat-sheet membranes from poly(vinylidene fluoride) for membrane distillation. *Desalination*. 1996;104(1–2):1–11.
33. Wang P, Luo L, Chung T-S. Tri-bore ultra-filtration hollow fiber membranes with a novel triangle-shape outer geometry. *J Membr Sci*. 2014;452:212–218.
34. Wang D, Li K, Teo WK. Porous PVDF asymmetric hollow fiber membranes prepared with the use of small molecular additives. *J Membr Sci*. 2000;178(1–2):13–23.
35. Fan H, Peng Y. Application of PVDF membranes in desalination and comparison of the VMD and DCMD processes. *Chem Eng Sci*. 2012;79:94–102.
36. Tomaszewska M. Membrane distillation. *Environ Prot Eng*. 1999;25(1):37–47.
37. Khayet M. Membranes and theoretical modeling of membrane distillation: a review. *Adv Colloid Interface Sci*. 2010;164(1–2):56–88.
38. Song LM, Ma ZD, Liao XH, Kosaraju PB, Irish JR, Sirkar KK. Pilot plant studies of novel membranes and devices for direct contact membrane distillation-based desalination. *J Membr Sci*. 2008;323(2):257–270.
39. Teoh MM, Peng N, Chung TS, Koo LL. Development of novel multichannel rectangular membranes with grooved outer selective surface for membrane distillation. *Ind Eng Chem Res*. 2011;50(24):14046–14054.
40. Bonyadi S, Chung TS, Rajagopalan R. A novel approach to fabricate macrovoid-free and highly permeable PVDF hollow fiber membranes for membrane distillation. *AIChE J*. 2009;55(3):828–833.
41. Tang Y, Li N, Liu A, Ding S, Yi C, Liu H. Effect of spinning conditions on the structure and performance of hydrophobic PVDF hollow fiber membranes for membrane distillation. *Desalination*. 2012;287:326–339.
42. Wu B, Li K, Te WK. Preparation and characterization of poly(vinylidene fluoride) hollow fiber membranes for vacuum membrane distillation. *J Appl Polym Sci*. 2007;106(3):1482–1495.
43. Lui A, Talbot FDF, Fouda A, Matsuura T, Sourirajan S. Studies on the solvent exchange technique for making dry cellulose acetate membranes for the separation of gaseous mixtures. *J Appl Polym Sci*. 1988;36(8):1809–1820.
44. Yang TX, Shi GM, Chung TS. Symmetric and asymmetric zeolitic imidazolate frameworks (ZIFs)/polybenzimidazole (PBI) nanocomposite membranes for hydrogen purification at high temperatures. *Adv Energy Mater*. 2012;2(1–2):1358–1367.
45. Park HC, Moon YS, Rhee HW, Kang YS, Kim UY. Effect of solvent exchange on the morphology of asymmetric membranes. In: Pinnau I, Freeman BD, editors. Membrane Formation and Modification. ACS, Washington, DC, 1999.
46. Perry RH. *Perry's Chemical Engineering Handbook*, *6th ed*. Singapore: McGraw-Hill Book, 1984.
47. Garcia-Payo MC, Izquierdo-Gil MA, Fernandez-Pineda C. Wetting study of hydrophobic membranes via liquid entry pressure measurements with aqueous alcohol solutions. *J Colloid Interface Sci*. 2000;230(2):420–431.
48. Qi B, Li B, Wang S. Investigation of shell side heat transfer in cross-flow designed vacuum membrane distillation module. *Ind Eng Chem Res*. 2012;51(35):11463–11472.
49. Chuang CJ, Tung KL, Fan YH, Ho CD, Huang J. Performance evaluation of ePTFE and PVDF flat-sheet module direct contact membrane distillation. *Water Sci Technol*. 2010;62(2):347–352.
50. Phattaranawik J, Jiraratananon R, Fane AG. Effect of pore size distribution and air flux on mass transport in direct contact membrane distillation. *J Membr Sci*. 2003;215(1–2):75–85.
51. Mericq JP, Laborie S, Cabassud C. Evaluation of systems coupling vacuum membrane distillation and solar energy for seawater desalination. *Chem Eng J*. 2011;166(2):596–606.
52. He F, Gilron J, Lee H, Song L, Sirkar KK. Studies on scaling of membranes in desalination by DCMD: $CaCO_3$ and mixed $CaCO_3$/$CaSO_4$ systems. *Chem Eng Sci*. 2009;64(8):1844–1859.
53. Chen H, Wu C, Jia Y, Wang X, Lu X. Comparison of three membrane distillation configurations and seawater desalination by vacuum membrane distillation. *Desalination Water Treat*. 2011;28(1–3):321–327.
54. Zhang J, Li JD, Duke M, Xie Z, Gray S. Performance of asymmetric hollow fibre membranes in membrane distillation under various configurations and vacuum enhancement. *J Membr Sci*. 2010;362(1–2):517–528.

Manuscript received Apr. 24, 2013, and revision received Dec. 2, 2013.